data points lying slightly to the left of the psychometric data points; in this case the neuronal threshold was slightly lower than the psychophysical one. We used a likelihood-ratio statistic to test the hypothesis that the psychometric and neurometric functions were the same. For this neuron, this hypothesis could not be rejected ($P > 0.05$).

We performed this analysis for 45 neurons recorded from one monkey, and 15 neurons from a second. Figure 2 shows a histogram of the distribution of the ratio of neurometric to psychometric thresholds for these 60 neurons. Values of this ratio of <1 represent cases where the neuron's threshold was lower than the monkey's; values >1 represent cases where the monkey's performance was better than the neuron's. Intuitively, it might be expected that the behavioural threshold would be lower than any particular neuronal threshold but, in most cases, neuronal thresholds and perceptual thresholds were similar. Indeed in some cases, neuronal thresholds were substantially *lower* than perceptual thresholds. For 20 of the 60 neurons in our sample, the psychometric and neurometric functions were statistically indistinguishable ($P > 0.05$); in 18 of the 40 remaining cases, neuronal thresholds were lower than perceptual thresholds. In other words, if the monkeys were able to select and measure the discharge of some of these neurons as we did, their performance could have been better than it actually was.

An inability to select the most informative signals can be considered as a kind of perceptual uncertainty, of the kind modelled by Pelli[13]. Obliged to monitor signals from many sources less informative than the one perfectly tuned to the visual target, the animal's perceptual performance would be degraded, because each sub-optimal source would contribute more noise than signal. Neuronal performance would then exceed psychophysical performance. Our results suggest, however, that this effect is not large. Substantial uncertainty would make the psychometric function steeper than the neurometric function[13], but as was the case for the example shown in Fig. 1*b*, the slopes of these two functions are usually similar. We thus conclude that under our conditions, the monkey's perceptual decision is not greatly affected by irrelevant signals introduced by uncertainty.

The apparent absence of uncertainty leads, however, to another question: if a perceptual decision can be based with relative certainty on the discharge of the most informative neurons, why is behavioural performance not further enhanced by using a pooled signal derived from many such informative neurons? If enough such neurons were present, such pooling would substantially improve psychophysical performance by averaging out the noise that obscures weak signals. Our data show that in most cases, the neuronal and psychophysical performances are similar, indicating that signals from many neuronal sources are not pooled to reduce perceptual thresholds.

One way to account for the absence of either pooling or uncertainty effects is to suggest that the variability in the responses of similarly tuned neurons is correlated. Both pooling and uncertainty act as we have stated only if different neuronal signals are perturbed by *independent* sources of variation. If the sources are not independent, then uncertainty does no damage and pooling provides no benefit, because different neurons are carrying similar signals. The rich network of shared connections that link MT neurons with the retina might well produce correlation among neurons with related selectivities, but this possibility has not been studied. Our lack of information about the degree of shared variability makes it impossible for us to assert that the neurons whose responses we have recorded are the ones that contribute to the monkey's perceptual judgements. Nonetheless, our results show that a reasonable account of the monkey's performance can be constructed, using a simple decision rule, from signals carried by small numbers of neurons whose selectivities are well matched to the demands of the perceptual task. □

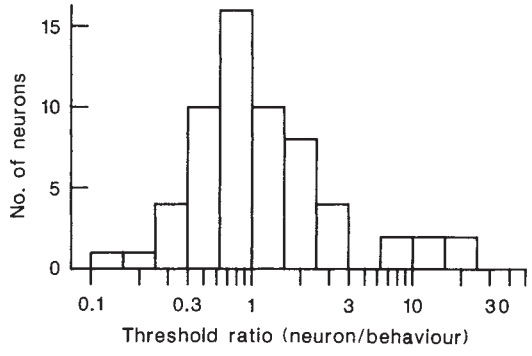

FIG. 2 Comparison of psychophysical and physiological thresholds obtained for 60 MT neurons in two rhesus monkeys. The frequency histogram shows the distribution of the ratio of the physiological threshold to the psychophysical threshold for all the neurons for which we obtained data. A value of 1 represents perfect correspondence between psychophysical and physiological thresholds; values <1 indicate that the physiological threshold was lower than the psychophysical threshold, whereas values >1 indicate the converse. The directional preferences of the 60 neurons were roughly uniformly distributed, and there was no reliable association between a neuron's direction or speed preference and its threshold relative to the perceptual threshold.

Received 10 April; accepted 25 July 1989.

1. Barlow, H. B. & Levick, W. R. *J. Physiol.* **200,** 1–24 (1969).
2. Tolhurst, D. J., Movshon, J. A. & Dean, A. F. *Vision Res.* **23,** 775–785 (1983).
3. Parker, A. J. & Hawken, M. J. *J. opt. Soc. Am.* **A2,** 1101–1114 (1985).
4. Bradley, A., Skottun, B. C., Ohzawa, I., Sclar, G. & Freeman, R. D. *J. Neurophysiol.* **57,** 755–772 (1987).
5. Mikami, A., Newsome, W. T. & Wurtz, R. H. *J. Neurophysiol.* **55,** 1308–1327 (1986).
6. Newsome, W. T. & Paré, E. B. *J. Neurosci.* **8,** 2201–2211 (1988).
7. Dubner, R. & Zeki, S. M. *Brain Res.* **35,** 528–532 (1971).
8. Zeki, S. M. *J. Physiol.* **236,** 549–573 (1974).
9. Maunsell, J. H. R. & Van Essen, D. C. *J. Neurophysiol.* **49,** 1127–1147 (1983).
10. Albright, T. D. *J. Neurophysiol.* **52,** 1106–1130 (1984).
11. Green, D. M. & Swets, J. A. *Signal Detection Theory and Psychophysics.* (Wiley, New York, 1966).
12. Quick, R. F. *Kybernetik* **16,** 65–67 (1974).
13. Pelli, D. G. *J. opt. Soc. Am.* **A2,** 1508–1532 (1985).

ACKNOWLEDGEMENTS. This work was supported by grants from NIH and by a Sloan Research Fellowship to W.T.N.

Hippocampal abnormalities in amnesic patients revealed by high-resolution magnetic resonance imaging

G. A. Press*, D. G. Amaral† & L. R. Squire‡

* Department of Radiology and Magnetic Resonance Institute, University of California, School of Medicine, San Diego, California 92103, USA
† The Salk Institute, La Jolla, California 92037, USA
‡ Department of Psychiatry, University of California, School of Medicine and Veterans Administration Medical Center, San Diego, California 92161, USA

THE identification of brain structures and connections involved in memory functions has depended largely on clinico-pathological studies of memory-impaired patients[1–4], and more recently on studies of a primate model of human amnesia[5,6]. But quantitative neurobehavioural data and detailed neuropathological information are rarely available for the same patients[7–9]. One case has demonstrated that selective bilateral damage to the hippocampus causes a circumscribed memory impairment in the absence of other intellectual deficits[9]. This finding, in conjunction with evidence from humans[10,11] and monkeys[12–16], indicates that the hippocampus together with adjacent and anatomically related structures is essential for the formation of long-term memory, perhaps by virtue of

TABLE 1 Subject characteristics

Patient	Age (yr)	WAIS-R	WMS-R				
			Attention/conc.	Verbal	Visual	General	Delay
Controls							
1	65	103	92	96	109	102	102
2	70	110	111	91	93	89	100
3	57	119	114	114	120	121	138
4	63	137	124	125	123	129	138
Mean	63.8	117.3	110.3	106.5	111.3	110.3	119.5
Amnesics							
W.H.	66	113	88	72	82	67	<50
J.L.	69	116	122	73	83	74	58
L.M.	58	111	132	87	96	90	65
Mean	64.3	113.3	114.0	77.3	87.0	77.0	57.7

WAIS-R, Wechsler Adult Intelligence Scale-Revised; WMR-R, Wechsler Memory Scale-Revised. The WAIS-R and each of the five indices of the WMS-R yield a mean score of 100 in the normal population with a standard deviation of 15. The WMS-R does not provide numerical scores for subjects who score below 50. Therefore, the single value below 50 was scored as 50 for computing a group mean.

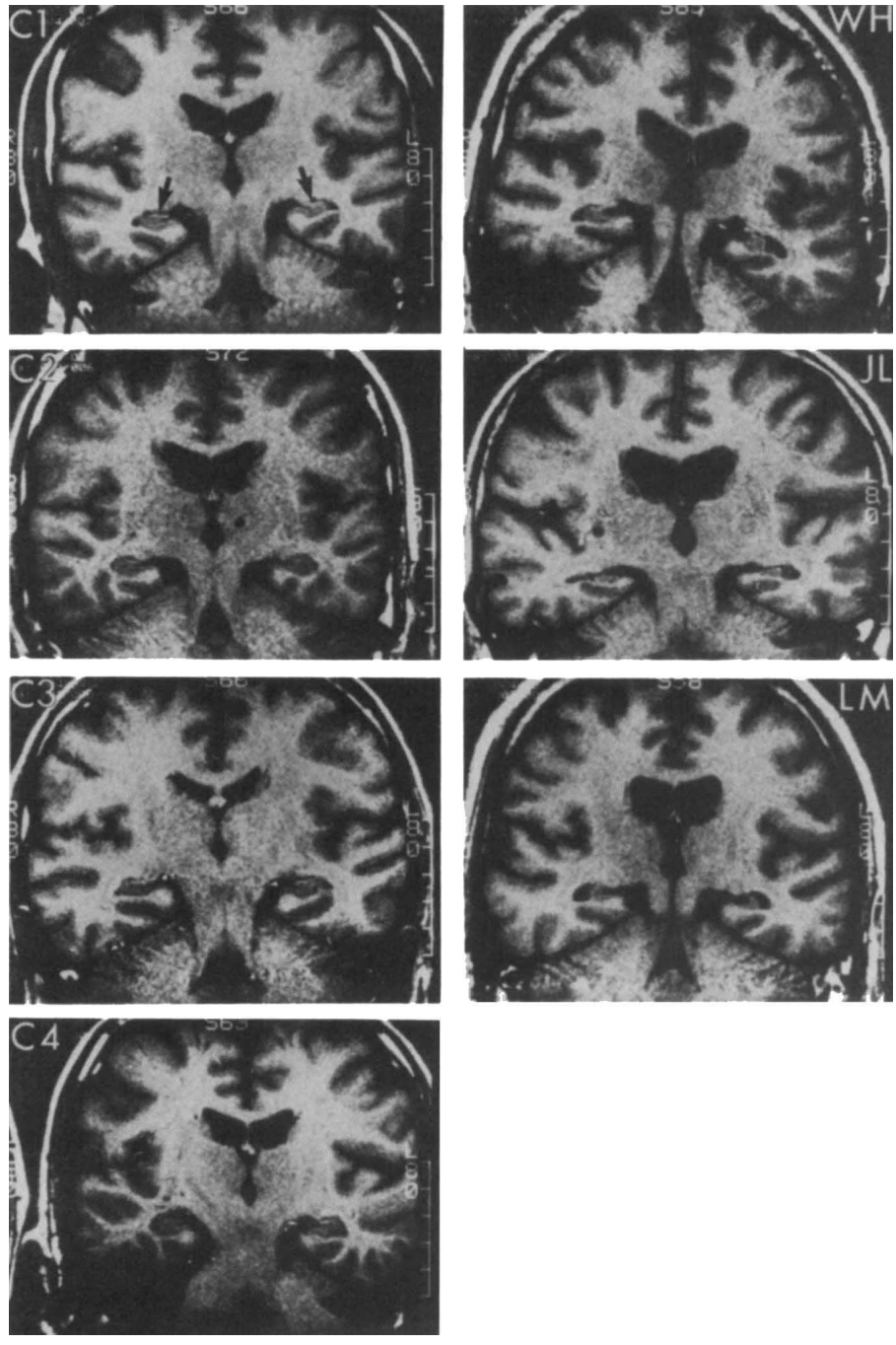

FIG. 1 T1-weighted (TE = 400 ms, TR = 20 ms) images of 5-mm thick slices through the hippocampal formation. These photographs show the first or second of the three levels through the hippocampal formation that were submitted to quantitative analysis. Panels on the left (C1–C4) show images from neurologically intact control subjects, and panels on the right show images from three amnesic patients (W.H., J.L. and L.M.). The area of the hippocampal formation (indicated by arrows in panel C1) in the amnesic patients averaged 49% of the corresponding area in control subjects. In contrast, the average area of the temporal lobe (measured from the fundus of the collateral sulcus to the inferior limiting sulcus) was nearly identical in the two groups. The parahippocampal gyrus is smaller in J.L. than in the other amnesic and control subjects. The photographs show the left side of the brain on the right side of each panel. The calibration bar at the right of each panel represents 5 cm in 1-cm increments.

the extensive reciprocal connections between the hippocampal formation and putative memory storage sites in the neocortex[17]. Although cognitive studies of amnesia provide useful information about the functional organization of normal memory[1,18–21], it has not usually been possible to relate memory impairment to anatomy in living patients. We have developed a high-resolution protocol for imaging the human hippocampus with magnetic resonance that permits visualization of the hippocampal formation in substantial cytoarchitectonic detail, revealing abnormalities in patients with severe and selective memory impairment.

Three male amnesic patients and four male control subjects were examined (Table 1). Patient W.H. became amnesic rapidly over the course of several days in 1986 without antecedent head trauma, seizure or unconsciousness. Patient J.L. became amnesic gradually during a period of about two years (from early 1985 to early 1987); his cognitive status has remained stable since that time. The aetiology in these two cases was unknown. Patient L.M. became amnesic in 1984 as the result of a respiratory arrest which occurred during an epileptic seizure. All three patients were severely impaired on standard tests of verbal and non-verbal memory[22,23]. For example, learning of 10 noun pairs across three trials[24] was 0.3, 0.3 and 1.0 pair (controls; 6.3, 7.5 and 8.5). The amnesic patients performed well on other cognitive tests, such as on the non-memory portions of the Dementia Rating Scale[25] (maximum score, 119; patients, 116.3; controls, 118.3) and on the Controlled Word Association Test (FAS)[26] (patients, 52.0 words; controls, 41.8 words).

Magnetic resonance examinations were performed with a 1.5-tesla superconducting magnet (General Electric, Milwaukee). In preliminary studies, we determined that the optimal resolution of the hippocampus was obtained when the hippocampus was imaged perpendicular to its long axis. Accordingly, each subject was supine on the magnetic resonance examination table within the magnet, and the head was tilted posteriorly so that the line joining the lips and the external auditory canal was perpendicular to the table (and the longitudinal axis of the magnetic field). A sagittal, T1-weighted (TR = 200 ms, TE = 20 ms, 1 excitation (NEX)) spin-echo sequence (field of view (FOV) = 24 cm, matrix = 256 × 128) centred at the mid-line showed the long axis of the hippocampus clearly. The head of the patient was then repositioned slightly if necessary to orientate the hippocampus appropriately. Coronal images were then obtained using a T1-weighted sequence (TR = 400 ms, TE = 20 ms, 6 NEX; FOV = 16, matrix = 256 × 256), which provided six interleaved, 5 mm-thick sections (no interslice gaps) with 0.625 mm in-plane spatial resolution. We obtained the first section just caudal to the pes hippocampus and were able to survey 30 mm of the hippocampus out of a total rostrocaudal length of 40 mm. Coronal proton-density and T2-weighted images (TR = 2,700 ms, TE = 30 and 80 ms, 1 or 2 NEX; FOV 16, matrix = 256 × 256) were also obtained.

The images obtained by our high-resolution, T1-weighted protocol showed the hippocampal formation in considerable detail (Figs 1 and 2). For example, Fig. 2*a* illustrates in a normal subject the pyramidal cell fields of the subiculum and hippocampus, the fimbria, perforant path, stratum lacunosum-moleculare, the alveus, and the molecular layer of the dentate gyrus. To calculate areal boundaries within the temporal lobes, we selected slices that were located at about the same rostrocaudal level in each subject. For each series of images, the first section caudal to the pes hippocampus and the two adjacent caudal sections were selected for analysis.

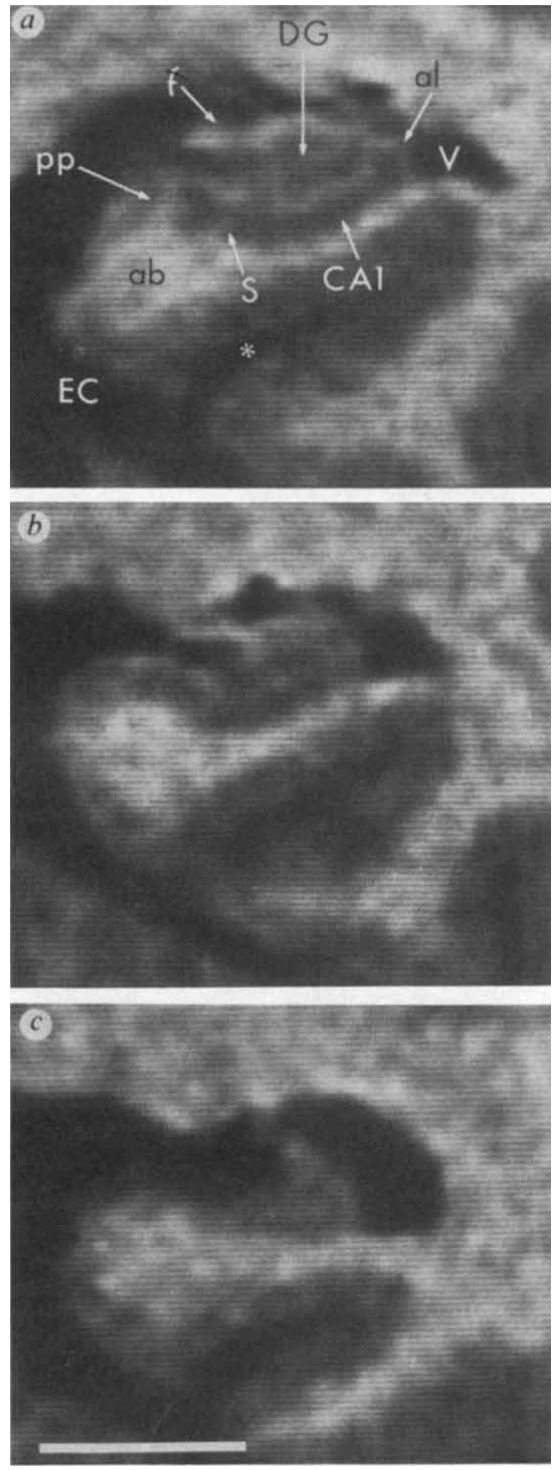

FIG. 2 Higher magnification magnetic resonance images than those shown in Fig. 1 of the left hippocampal formation. *a*, T1-weighted image (TE = 400 ms, TR = 20 ms) of a 5-mm thick section through the hippocampal formation of a 24-year-old normal subject. It is possible to distinguish the angular bundle (ab), the perforant path (pp), the alveus (al), the molecular layer of the dentate gyrus (DG), and the fimbria (f). The pyramidal cell layer of the subiculum (S) and the CA1 field of the hippocampus (which are ~1.5-mm thick in the coronal plane at this level) can also be seen. The entorhinal cortex (EC) lies just ventral to the angular bundle. The region of high signal intensity superficial to the pyramidal cell layer marks the stratum lacunosum-moleculare, in which the perforant path projects to the hippocampus and dentate gyrus. The temporal horn of the lateral ventricle (V) lies just lateral and dorsal to the hippocampus, and the asterisk marks the position of the collateral sulcus. *b*, Hippocampal formation of control subject C1 at the same level seen in Fig. 2. Whereas this image is not as distinct as the one from the younger subject, most of the anatomical features identified in that image can also be distinguished here. *c*, Hippocampal formation of amnesic patient L.M. at the same level as in Fig. 1. In contrast to the images in *a* and *b*, the fimbria is not distinct in this image, and it is difficult to determine the boundary of the pyramidal cell layer in the subiculum or hippocampus. In addition, there is marked reduction of the size of the dentate gyrus, hippocampus, and subiculum. The calibration bar represents 1 cm in all three panels.

Using 11 × 14 inch photographs and a microcomputer-linked digitizing tablet, the area of the hippocampal formation (defined as the fimbria, dentate gyrus, hippocampus proper and subiculum) was computed on each side and in each of the three sections. We then measured the combined area of the hippocampal formation and the parahippocampal gyrus (extending from the subiculum to the fundus of the collateral sulcus) and the area of each temporal lobe (minus the hippocampal formation and parahippocampal gyrus). The outline for the temporal lobe measurement extended from the fundus of the collateral sulcus to the inferior limiting sulcus of the insular cortex. The left and right lateral ventricles and the third ventricle were also measured. We expressed the area of each of the regions as the average per section of the areal values for the sampled sections.

The area of the temporal lobe was nearly identical in the two groups (controls: left temporal lobe, 11.57 cm^2, right temporal lobe, 12.75 cm^2; patients: left temporal lobe, 11.85 cm^2, right temporal lobe, 13.57 cm^2). By contrast, the hippocampal formation (HF) in the patients was markedly reduced in size (controls: left HF, 0.60 cm^2, right HF, 0.67 cm^2; patients: left HF, 0.29 cm^2, right HF, 0.33 cm^2). The area of the hippocampal formation in the patients was 49% of that in the control subjects ($t_5 = 5.4$, $P < 0.01$). The results were the same when the area of the hippocampal formation was calculated as a percentage of the size of the temporal lobe (controls, 5.3%, patients, 2.5%). The lateral ventricles (patients, 4.31 cm^2; controls, 2.84 cm^2) and the third ventricle (patients; 1.05 cm^2; controls, 0.76 cm^2) were somewhat larger in the patients than in the controls, but these differences were not significant ($0.1 > P < 0.05$). Patient J.L. had left and right ventricles outside the normal range; patients J.L. and L.M. had third ventricles outside the normal range. Finally, the area of the parahippocampal gyrus was smaller in patient J.L. (the average area of each side was 1.01 cm^2, or 7.5% of the area of the temporal lobe). The parahippocampal area was nearly the same in the other two amnesic patients as in the control subjects (patients: 1.29 cm^2, 10.5% of the temporal lobe area; controls: 1.28 cm^2, 10.5% of the temporal lobe area).

T2-weighted images revealed no regions of abnormal signal intensity in the brain of patient L.M. The other two patients had non-specific, abnormal, hyper-intense foci in the striatum, as previously reported; for example, in ischaemia, de-myelination, or infarction[27]. Patient J.L. had several additional hyper-intense foci distributed in the white matter.

This high-resolution magnetic resonance protocol focused on one area of interest and did not survey all brain regions. Accordingly, we cannot exclude the possibility that additional abnormalities might have been detected if other areas had been surveyed as carefully as the hippocampal formation. Nevertheless, circumscribed memory impairment has been associated previously with histologically confirmed hippocampal lesions in the absence of other significant damage[9], so the abnormalities that we have identified are likely to have contributed substantially to memory dysfunction in all three patients.

Our magnetic resonance protocol has acquired images with a better resolution of the hippocampal formation than is obtained by more standard protocols[28–30]. We attribute this improved resolution to the fact that we obtained images precisely perpendicular to the long axis of the hippocampus. Because damage to the hippocampal formation occurs prominently in Alzheimer's disease[31], and memory impairment is one of its earliest symptoms, this protocol might be useful in achieving an early diagnosis of the disease. □

Received 29 May; accepted 7 August 1989.

1. Squire, L. R. *Memory and Brain* (Oxford University Press, New York, 1987).
2. Damasio, A. R. *Semin. Neurol.* **4,** 223–225 (1986).
3. Markowitsch, H. J. *Brain Res. Rev.* **13,** 351–370 (1988).
4. Victor, M., Adams, R. & Collins, G. H. *The Wernicke-Korsakoff Syndrome and Related Neurologic Disorders due to Alcoholism and Malnutrition* (2nd edn) (Davis, Philadelphia, 1989).
5. Mishkin, M., Spiegler, J., Saunders, R. C. & Malamut, B. J. in *Toward a Treatment of Alzheimer's Disease* (eds Corkin, S., Davis, K. L., Growdon, J. H., Usdin, E. J. & Wurtman, R. J.) 235–247 (Raven, New York, 1982).
6. Squire, L. R. & Zola-Morgan, S. in *The Physiological Basis of Memory* (ed. Deutsch, J. A.) 199–268 (Academic, New York, 1983).
7. Mair, W. G. P., Warrington, E. K. & Weiskrantz, L. *Brain* **102,** 749–783 (1979).
8. Mayes, A. R., Meudell, P. R., Mann, D. & Pickering, A. *Cortex* **24,** 367–388 (1988).
9. Zola-Morgan, S., Squire, L. R. & Amaral, D. G. *J. Neurosci.* **6,** 2950–2967 (1986).
10. Scoville, W. B. & Milner, B. *J. Neurol. Neurosurg. Psychiat.* **20,** 11–21 (1957).
11. Victor, M., Angevine, J. & Fisher, C. M. *Archs. Neurol.* **5,** 244–263 (1961).
12. Mishkin, M. *Nature* **273,** 297–298 (1978).
13. Mahut, H., Zola-Morgan, S. & Moss, M. J. *J. Neurosci.* **2,** 1214–1229 (1982).
14. Zola-Morgan, S., Squire, L. R. & Amaral, D. G. *J. Neurosci.* **9,** 898–913 (1989).
15. Zola-Morgan, S., Squire, L. R. & Amaral, D. G. *J. Neurosci.* (in the press).
16. Zola-Morgan, S., Squire, L. R., Amaral, D. G. & Suzuki, W. A. *J. Neurosci.* **9,** 1922–1936 (1989).
17. Squire, L. R., Shimamura, A. P. & Amaral, D. G. in *Neural Models of Plasticity* (eds Byrne, J. & Berry, W.) 208–239 (Academic, New York, 1989).
18. Weiskrantz, L. *Human Neurobiol.* **6,** 93–105 (1987).
19. Baddeley, A. *Trends Neurosci.* **11,** 176–181 (1988).
20. Schacter, D. L. in *Memory Systems of the Brain: Animal and Human Cognitive Processes* (eds Weinberger, N., Lynch, G. & McGaugh, J.) 351–379 (Guilford, New York, 1985).
21. Shimamura, A. P. in *Handbook of Neuropsychology* (eds Boller, F. & Grafman, J.) (Elsevier, Amsterdam, in the press).
22. Squire, L. R. & Shimamura, A. P. *Behavl Neurosci.* **100,** 866–877 (1986).
23. Janowsky, J. S., Shimamura, A. P., Kritchevsky, M. & Squire, L. R. *Behavl Neurosci.* **103,** 548–560 (1989).
24. Jones, M. K. *Neuropsychologia* **12,** 21–30 (1974).
25. Mattis, S. in *Geriatric Psychiatry* (eds Bellack, R. & Karasu, B.) 77–121 (Grune & Stratton, New York, 1976).
26. Benton, A. L. & Hamsher, K. *Multilingual Aphasia Examination* (Univ. Iowa, Iowa City, 1976).
27. Braffman, B. H. *et al. Am. J. Neuroradiol.* **9,** 629–636 (1988).
28. Seab, J. P. *et al. Magnetic Resonance in Medicine* **8,** 200–208 (1988).
29. Nadich, T. P. *et al. Radiology* **162,** 747–754 (1987).
30. Jack, C. R. *et al. Radiology* **172,** 549–554 (1989).
31. Hyman, B. T., Van Hoesen, G. W., Damasio, A. R. & Barnes, C. L. *Science* **225,** 1168–1170 (1984).

ACKNOWLEDGEMENTS. We thank Dr B. Schwaighofer, J. Zouzounis, P. Hoover and M. Arzaga for assistance. This work was supported bythe Medical Research Service of the Veterans Administration, the NIMH, the NINCDS, the McKnight Foundation, the Office of Naval Research, and a Bioscience Grant for International Joint Research from the NEDO, Japan.

Intercellular adhesion molecule-1 is an endothelial cell adhesion receptor for *Plasmodium falciparum*

A. R. Berendt, D. L. Simmons*, J. Tansey, C. I. Newbold & K. Marsh

Molecular Parasitology Group and * Imperial Cancer Research Fund, Institute of Molecular Medicine, University of Oxford, John Radcliffe Hospital, Headington, Oxford OX3 9DU, UK

THE primary event in the pathogenesis of severe malaria in *Plasmodium falciparum* infection is thought to be adherence of trophozoite- and schizont-infected erythrocytes to capillary endothelium[1], a process called sequestration. Identifying the endothelial molecules used as receptors is an essential step in understanding this disease process. Recent work implicates the membrane glycoprotein CD36 (platelet glycoprotein IV; refs 2–5) and the multi-functional glycoprotein thrombospondin[6] as receptors. Although CD36 has a widespread distribution on microvascular endothelium[7], it may not be expressed on all capillary beds where sequestration occurs, especially in the brain[8]. The role of thrombospondin in cell adhesion, *in vitro* or *in vivo*, is less certain[4,9]. We have noticed that some parasites bind to human umbilical-vein endothelial cells independently of CD36 or thrombospondin. To screen for alternative receptors, we have developed a novel cell-adhesion assay using transfected COS cells, which confirms that CD36 is a cell-adhesion receptor. In addition, we find that an endothelial-binding line of *P. falciparum* binds to COS cells transfected with a complementary DNA encoding intercellular adhesion molecule-1. As this molecule is widely distributed on capillaries and is inducible[10], this finding may be relevant to the pathogenesis of severe malaria.

We have observed that binding of red blood cells infected with Gambian wild isolates of *P. falciparum*, in the C32 amelanotic melanoma cell adherence assay varies markedly, but does not correlate with severity of clinical malaria[11]. More